Nuclear Engineering and Technology 54 (2022) 193–206

Contents lists available at ScienceDirect

Nuclear Engineering and Technology

journal homepage: www.elsevier.com/locate/net

Original article

Localization and size estimation for breaks in nuclear power plants

Ting-Han Lin [a], Ching Chen [b], Shun-Chi Wu [a, b, *], Te-Chuan Wang [c], Yuh-Ming Ferng [a, b]

[a] Institute of Nuclear Engineering and Science, National Tsing Hua University, 101, Section 2 Kuang Fu Road, Hsinchu, 30013, Taiwan
[b] Department of Engineering and System Science, National Tsing Hua University, 101, Section 2 Kuang Fu Road, Hsinchu, 30013, Taiwan
[c] Institute of Nuclear Energy Research, Atomic Energy Council, R.O.C., 100, Wenhua Road, Jiaan Village, Longtan District, Taoyuan, 32546, Taiwan

ARTICLE INFO

Article history:
Received 17 December 2020
Received in revised form
1 July 2021
Accepted 4 July 2021
Available online 7 July 2021

Keywords:
Break localization
Break size estimation
Multiple signal classification (MUSIC)
Deep learning

ABSTRACT

Several algorithms for nuclear power plant (NPP) break event detection, isolation, localization, and size estimation are proposed. A break event can be promptly detected and isolated after its occurrence by simultaneously monitoring changes in the sensing readings and by employing an interquartile range-based isolation scheme. By considering the multi-sensor data block of a break to be rank-one, it can be located as the position whose lead field vector is most orthogonal to the noise subspace of that data block using the Multiple Signal Classification (MUSIC) algorithm. Owing to the flexibility of deep neural networks in selecting the best regression model for the available data, we can estimate the break size using multiple-sensor recordings of the break regardless of the sensor types. The efficacy of the proposed algorithms was evaluated using the data generated by Maanshan NPP simulator. The experimental results demonstrated that the MUSIC method could distinguish two near breaks. However, if the two breaks were close and of small sizes, the MUSIC method might wrongly locate them. The break sizes estimated by the proposed deep learning model were close to their actual values, but relative errors of more than 8% were seen while estimating small breaks' sizes.

1. Introduction

Break events in nuclear power plants (NPPs) can result in a loss of coolant or pressure or reduction in coolant flow rate. Furthermore, they can also result in reactor core damage if not effectively and instantly managed [1]. For example, the small-break loss-of-coolant accident (LOCA) in Three Mile Island was caused by inadvertently opening a power-operated relief valve. This resulted in a fuel meltdown in the reactor core owing to the operators failing to recognize this break for considerable length of time and taking inappropriate mitigation actions [2]. Thus, determining the break location and size in its early stage is essential to preempt a break event escalating into a severe accident [3]. One way to accomplish this is to examine the data tendencies from primary plant sensors by experienced operators. However, the high-level variation in the sensor readings may hinder this task. Therefore, avoiding mistakes in this manual approach is challenging, owing to the stressful and chaotic circumstances operators face [4]. To address this concern, a method that explores the relationship between a break event and the profile exhibiting among the NPP sensors for assessing the location and size of a break can be an alternative [3].

Examples of the aforementioned method include works based on artificial neural networks [5], probabilistic neural networks [6], and support vector machines [3,7]. Break localization is treated as a pattern recognition problem in these studies, as NPP sensors exhibit varying profiles for breaks at different locations. The differences among these cited studies include the classifiers employed and the methods for extracting event features to reduce noise effect and remove redundant information from multi-sensor data. Furthermore, efforts have been made to estimate the break size [3,8–10] for which approaches that provide continuous size estimates are commonly used [3,8,10]. Although rarely reported, discretization of the break size into several size scales (e.g., 20%, 40%, etc.) during size estimation has been employed [9]. Notably, the occurrence of breaks in most of these studies was detected during the triggering of the reactor scram [3,6,7]. Additionally, break events can also be detected by continuously monitoring the primary sensing variables in the reactor to verify if the corresponding thresholds are exceeded [5]. As the required information (e.g., break location and size) is obtained solely through analysis and interpretation of acquired data, this method is known as a data-driven method.

* Corresponding author. Institute of Nuclear Engineering and Science, National Tsing Hua University, 101, Section 2 Kuang Fu Road, Hsinchu, 30013, Taiwan.
E-mail address: shunchi.wu@mx.nthu.edu.tw (S.-C. Wu).

https://doi.org/10.1016/j.net.2021.07.007

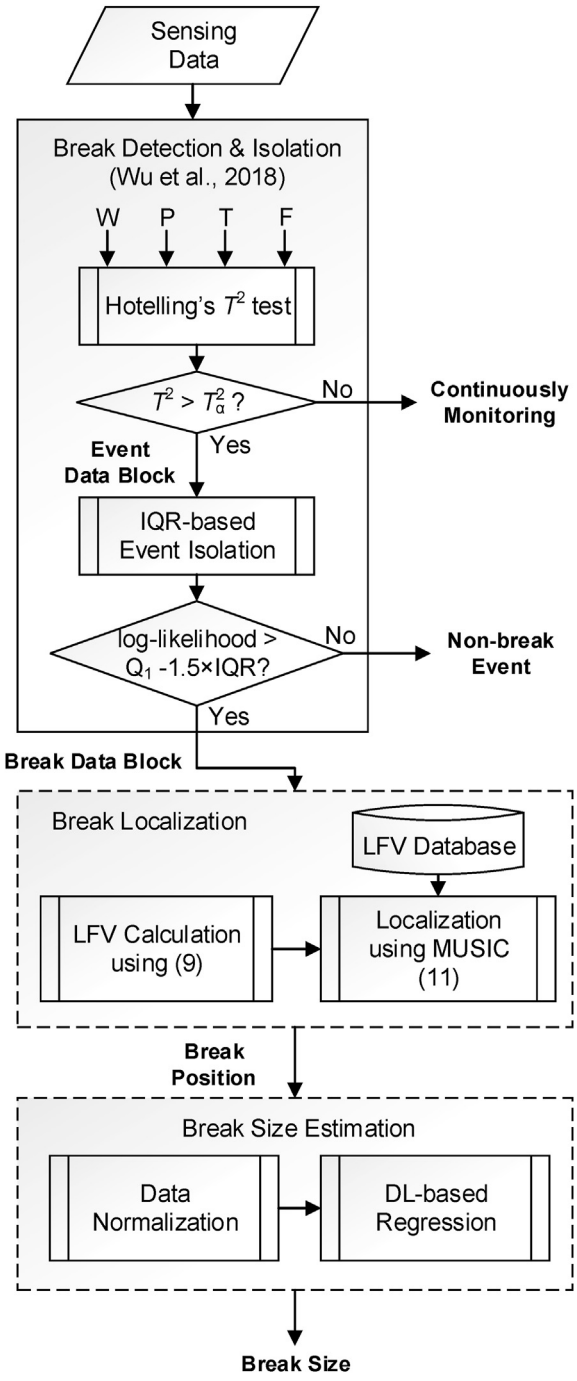

Fig. 1. System diagram of the proposed scheme. The dashed rectangles enclose the topics to be investigated in this study.

In this study, we focus on applying data-driven methods for break detection, isolation, localization, and size estimation in NPPs. Fig. 1 shows how these methods are employed in the proposed scheme. First, an algorithm that captures changes in the multi-sensor data is formulated to detect abnormal events. Based on Hotelling's T^2 test [11,12], the algorithm allows the detection threshold is determined without any empirical knowledge regarding the sensors. An interquartile range (IQR)-based isolation scheme is then applied to exclude a non-break event before localization [13]. Unlike existing approaches that rely on pattern recognition techniques for break localization, the proposed scheme applies the Multiple Signal Classification (MUSIC) method to the task. The MUSIC algorithm is based on the principle of subspace analysis and has been used for frequency estimation [14], radio direction finding [15], and brain source localization [16]. Given a set of lead field vectors (LFVs), the MUSIC algorithm determines the desired parameters (e.g., frequency of the signal of interest or location of a break) by searching for the parameter whose LFV is the most orthogonal to the noise subspace derived from the acquired data [16]. Furthermore, the MUSIC method is known for its high-resolution capability [17]; hence, two breaks having proper sizes that are close to each other can be distinguished. A deep learning-based approach is used for break size estimation. As the break size is a real value, its estimation is considered to be a regression problem. The simplest model for achieving this is linear regression. However, obtaining a hyper-plane that can fit the "data" (i.e., break sizes and sensor readings) is not easy, and the cost to estimate the regression coefficients of higher-order models can be high. By contrast, a deep neural network is a flexible model that adapts itself to the shape of the available data [18–20], and it can automatically select the best type of regression through training. Moreover, more hidden layers can be added to increase its prediction reliability. Finally, the network model weights can be efficiently determined using the backpropagation gradient descent algorithm [21].

The remainder of this paper is structured as follows. In the next section, we present approaches to detect and isolate a break. Section 3 describes locating a break using the MUSIC algorithm. The details of the deep learning model for break size estimation are given in Section 4. Generation of all the required data and the results of detailed experiments are provided in Section 5. Finally, some conclusions are presented in Section 6.

2. Break detection and isolation

An abnormal event (e.g., a break) in practice is not known until some indicator is evoked so that its localization and the recovery actions that follow can be commenced. This indicator might be the reactor scram [3,6,7], although, in the case of a small break event, a long time is required to trigger the scram. Any delay in recovery may cause inadequate core cooling, leading to core damage [1]. To enable prompt detection, continuously monitoring the reactor to observe if there is any abnormal change in sensing readings might be an alternative. Determining an abnormal change is achieved if a sensing variable exceeds its preset threshold [5,22,23]. However, such a threshold can be determined by empirical knowledge or the evaluation of plant operators. Another approach is to formulate the determination process as a hypothesis test. More specifically, $x(t)$ is the reading of a sensor at the time t, and whether it is taken under normal operation (i.e., the null hypothesis H_0) or an abnormal event (i.e., the alternative hypothesis H_1) is unknown:

$$\begin{aligned} H_0 &: x_0(t) = s(t) + w_0(t) \\ H_1 &: x_1(t) = s(t) + d(t) + w_1(t), \end{aligned} \tag{1}$$

The composites of $x(t)$ are different under two hypotheses. The additional term $d(t)$ appearing under the alternative hypothesis H_1 represents the signal that deviates from the normal operation signal $s(t)$ owing to an abnormal event. The white sensing noise $w_0(t)$ and $w_1(t)$ represent the noise under the null and alternative hypotheses, respectively. They are different but have the same statistical properties. Through deciding either to reject the null hypothesis in favor of the alternative or not reject it through, for example, Student's t-test [24], the occurrence of an abnormal event can be determined. Moreover, aided by the preset type I error (i.e., the null hypothesis wrongly rejected, typical values are 0.05 and 0.01), the two hypotheses can be distinguished without the need

for subjective reasoning.

To increase detection sensitivity, readings from more than one sensor are included. As such, the hypotheses in (1) should be generalized as

$$\begin{aligned} H_0 &: \mathbf{x}_0(t) = \mathbf{s}(t) + \mathbf{w}_0(t) \\ H_1 &: \mathbf{x}_1(t) = \mathbf{s}(t) + \mathbf{d}(t) + \mathbf{w}_1(t), \end{aligned} \tag{2}$$

where the vector $\mathbf{x}_0(t) = [x_{01}(t) \quad \cdots \quad x_{0m}(t)]^T \in \mathbb{R}^{m\times 1}$ comprises the readings of m sensors of the same type (e.g., pressure) under the null hypothesis at the time t, and the other terms in (2) are similarly defined. For the condition concerning the observation vector $\mathbf{x}(t)$, Hotelling's T^2 test is conducted. Note that Hotelling's T^2 statistic $T^2(t) = (\mathbf{x}(t) - \bar{\mathbf{x}}_0)^T \mathbf{G}_0^{-1} (\mathbf{x}(t) - \bar{\mathbf{x}}_0)$ follows a χ^2 distribution with m degrees of freedom, if $\mathbf{x}(t)$ is taken under the null hypothesis [11,12]. Finally, the sample covariance matrix

$$\mathbf{G}_0 = \frac{1}{n}\sum_{t=1}^{n}\left(\mathbf{x}_0(t) - \bar{\mathbf{x}}_0\right)\left(\mathbf{x}_0(t) - \bar{\mathbf{x}}_0\right)^T \in \mathbb{R}^{m\times m}, \tag{3}$$

is estimated using n data vectors collected under the null hypothesis, and $\bar{\mathbf{x}}_0$ is their ensemble average. The null hypothesis is rejected (i.e., the occurrence of a break) if the $T^2(t)$ value of any sensor type exceeds its corresponding threshold T_α^2, which can be determined under a given type [11,13].

The detection method mentioned above can detect any abnormal event. To isolate the break events of interest, an IQR-based isolation scheme is applied before localization. The idea is to consider a non-break event as an outlier to exclude [13]. An IQR is the difference between the first (Q_1) and third (Q_3) quartiles, defined as the values in the provided data series that contain 25% and 75% of the data below them, respectively. For the data to be classified as an outlier, it must have a value that lies outside the fence range from $Q_1 - 1.5 \times IQR$ to $Q_3 + 1.5 \times IQR$ [25]. To assign a data value to an abnormal event represented by the feature vector $\mathbf{f} \in \mathbb{R}^{p\times 1}$, the logarithm of the likelihood function $p(\mathbf{f}|\omega_B)$ of that event belonging to the break event class ω_B is used, and it is estimated by summing the Gaussian kernels centered at the n_B break event vectors $\mathbf{f}_i^B$ [26]:

$$p(\mathbf{f}|\omega_B) = \frac{1}{n_B}\sum_{i=1}^{n_B}\frac{1}{(2\pi)^{\frac{p}{2}}\sigma^p}\exp\left(-\frac{\left(\mathbf{f}-\mathbf{f}_i^B\right)^T\left(\mathbf{f}-\mathbf{f}_i^B\right)}{2\sigma^2}\right), \tag{4}$$

where σ is the smooth parameter that determines the width of a kernel function. Once obtained, the logarithm of the likelihood function determines whether it belongs to the break event class, or simply an outlier (i.e., a non-break event). Since it is unnecessary to consider an abnormal event whose logarithm of the likelihood function is higher than the upper value $Q_3 + 1.5 \times IQR$ to be a non-break event, we only check if the logarithm of the likelihood function is below the lower value $Q_1 - 1.5 \times IQR$. If so, this abnormal event is regarded as a non-break event. Finally, the feature vector used to represent an abnormal event for break event isolation can be extracted by techniques, such as the time integration method [3,6,7].

3. Break localization

3.1. Data stack and lead field vector

Using the model discussed in the previous section, the data vectors collected at n time instants (starting at the time when Hotelling's T^2 test-based approach detects the break) from m sensors of the same type are stacked as an $m \times n$ data block, $\mathbf{X} = [\mathbf{x}(1) \ \cdots \ \mathbf{x}(n)]$. The value of m is typically less than n (e.g., m = 9 and n = 61). We assume that for a set of sensors of the same type at different locations in the NPP, a break is regarded as a "point source," whose correctness is demonstrated in Section 5.2. Therefore, an appropriate mathematical model for X is

$$\mathbf{X} = \mathbf{a}\mathbf{v}^T + \mathbf{W} = \mathbf{S} + \mathbf{W}, \tag{5}$$

where $\mathbf{a} \in \mathbb{R}^{m\times 1}$ is referred to as the LFV of the break, $\mathbf{v} \in \mathbb{R}^{n\times 1}$ corresponds to the "signal" that the break generates, and $\mathbf{W} \in \mathbb{R}^{m\times n}$ is composed of the background and sensor noise, assumed to be white. Although the signal $\mathbf{S}$ is represented by an $m \times n$ matrix, it is the outer product of two vectors $\mathbf{a}$ and $\mathbf{v}$, and thus $\mathbf{S}$ is of rank one. An LFV is the response vector induced on the m-sensor array by a break signal of unit magnitude. As the response of a break induced on a sensor depends on the distance between them, breaks at different locations will have different LFVs, as shown in Fig. 2(a). To avoid scaling ambiguity in (5) (i.e., $c\mathbf{a}$ and $\mathbf{v}/c$ yield the same $\mathbf{X}$ as $\mathbf{a}$ and $\mathbf{v}$ for an arbitrary constant, c), the following conditions are employed: (1) $\|\mathbf{a}\|$ is equated to one, and (2) its first element should be positive. Furthermore, the LFVs of a break having different sizes are different, as shown in Fig. 2(b). When a break is large enough, it will significantly affect the sensors that do not respond when the break is small. This is found in Fig. 2(b) wherein the LFV elements of the flow rate sensors 1, and 7-10 become smaller owing to decreases in the flow rates at the sensor positions.

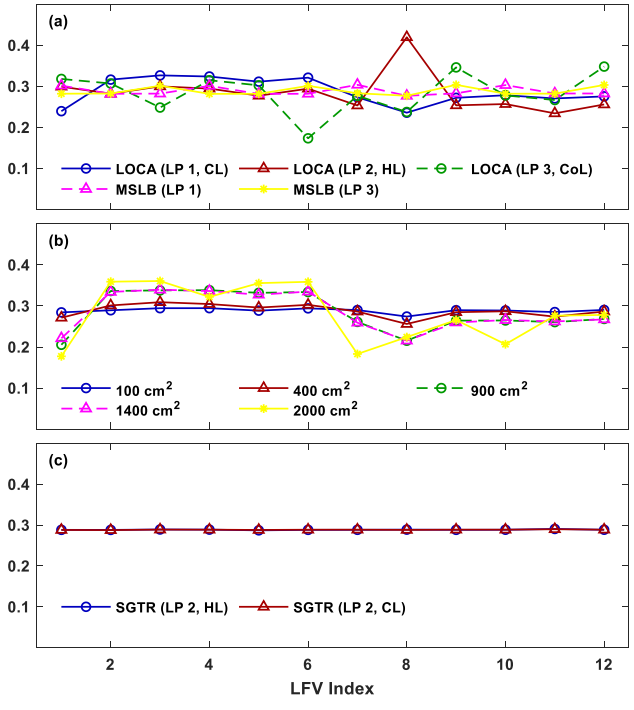

Fig. 2. The LFVs of various break events derived from their flow rate data blocks. (a) The LFVs of the breaks having the same size (1000 cm^2) at the cold leg of loop 1, the hot leg of loop 2, the crossover leg of loop 3, loop 1 of the main steam line, and loop 3 of the main steam line. (b) The LFVs of a break at the cold leg of loop 1 with its size varying from 100 cm^2 (1.3048%), 400 cm^2 (5.2192%), 900 cm^2 (11.7432%), 1400 cm^2 (18.2672%) to 2000 cm^2 (26.0960%). (c) The LFVs of the breaks at the hot leg side of steam generator tubes (loop 2) and cold leg side of steam generator tubes (loop 2) (i.e., Classes 15 and 16).

As $||\mathbf{a}|| = 1$, elements other than those previously mentioned increase accordingly. Thus, we may have the LFV of a break altered by changing its size.

To obtain the LFV of a break, we determine the best approximation to the noise-free multi-sensor signal, $\mathbf{S} = \mathbf{a}\mathbf{v}^T$, provided if data block $\mathbf{X}$ is available. Then, the break signal can be expressed as $\mathbf{v} = \mathbf{\Phi}\mathbf{c}$, with $\mathbf{\Phi} \in \mathbb{R}^{n\times n}$ and $\mathbf{c} \in \mathbb{R}^{n\times 1}$ being a chosen orthonormal basis (e.g., an identity matrix or a discrete wavelet transform basis matrix) and the corresponding coefficient vector, respectively. Next, data matrix $\mathbf{X}$ is vectorized to obtain the following [27]:

$$\mathbf{x} = \mathbf{v} \otimes \mathbf{a} + \mathbf{w} = \mathbf{\Phi}\mathbf{c} \otimes \mathbf{a} + \mathbf{w} = (\mathbf{\Phi} \otimes \mathbf{a})\mathbf{c} + \mathbf{w}, \tag{6}$$

where $\otimes$ denotes the Kronecker product, and $\mathbf{x}$, $\mathbf{s}$, and $\mathbf{w}$ are $mn \times 1$ vectors formed by vectorizing $\mathbf{X}$, $\mathbf{S}$, and $\mathbf{W}$, respectively. The LFV is obtained by correlating the known signal template (i.e., $\mathbf{s} = (\mathbf{\Phi} \otimes \mathbf{a})\mathbf{c}$) with noisy data $\mathbf{x}$:

$$\widehat{\mathbf{a}} = \arg\max_{\mathbf{a}} ||\mathbf{s}^T\mathbf{x}|| \text{ s.t. } ||\mathbf{a}|| = 1. \tag{7}$$

As

$$||\mathbf{s}^T\mathbf{x}||^2 = ||[(\mathbf{\Phi}\otimes\mathbf{a})\mathbf{c}]^T\mathbf{x}||^2 = \mathbf{c}^T\mathbf{y}(\mathbf{a})[\mathbf{y}(\mathbf{a})]^T\mathbf{c}, \tag{8}$$

where $\mathbf{y}(\mathbf{a}) = \mathbf{\Phi}^T\mathbf{X}^T\mathbf{a}$, the closed-form solution for $\mathbf{c}$ (in terms of $\mathbf{a}$) is $\mathbf{c} = \mathbf{y}(\mathbf{a})$, based on the Cauchy-Schwarz inequality. By replacing $\mathbf{c}$ with $\mathbf{\Phi}^T\mathbf{X}^T\mathbf{a}$, the original optimization problem of (7) becomes:

$$\widehat{\mathbf{a}} = \arg\max_{\mathbf{a}} ||\mathbf{y}(\mathbf{a})|| = \arg\max_{\mathbf{a}} ||\mathbf{a}^T\mathbf{X}|| \text{ s.t. } ||\mathbf{a}|| = 1. \tag{9}$$

The second equality holds owing to the vector norm-preserving property of orthogonal matrices. As (9) is in a quadratic form, $\widehat{\mathbf{a}}$ is determined as the left singular vector of $\mathbf{X}$ corresponding to the largest singular value. Once $\widehat{\mathbf{a}}$ is obtained, coefficient vector $\mathbf{c}$ is calculated as $\widehat{\mathbf{c}} = \mathbf{y}(\widehat{\mathbf{a}}) = \mathbf{\Phi}^T\mathbf{X}^T\widehat{\mathbf{a}}$, and $\widehat{\mathbf{v}} = \mathbf{\Phi}\widehat{\mathbf{c}} = \mathbf{X}^T\widehat{\mathbf{a}}$, which is the weighted sum of the rows of $\mathbf{X}$ with the weights being the entries of $\widehat{\mathbf{a}}$.

3.2. Multiple Signal Classification (MUSIC)

To locate a break, we first decompose its data block $\mathbf{X}$ using the singular value decomposition (SVD) method as follows:

$$\mathbf{X} = \mathbf{U}\Sigma\mathbf{V}^T = [\mathbf{u}_1 \quad \cdots \quad \mathbf{u}_m]\Sigma\mathbf{V}^T, \tag{10}$$

where $\mathbf{U}$ is an $m \times m$ orthonormal matrix composed of a set of orthonormal vectors, $\mathbf{u}_i$. Recall that $\mathbf{u}_1$, the left singular vector of $\mathbf{X}$ corresponding to the largest singular value, is the optimal estimate for the LFV of the unknown break. This indicates that the signal resides in the subspace spanned by $\mathbf{u}_1$, which is usually called the "signal subspace." As the signal $\mathbf{S}$ is of rank one and resides in the signal subspace spanned by $\mathbf{u}_1$, the subspace spanned by $\mathbf{u}_2 \ldots \mathbf{u}_m$ will have no signal but will contain noise. This latter subspace is thus referred to as the "noise subspace." As any other vector $\mathbf{u}_i$ is orthogonal to $\mathbf{u}_1$, $\mathbf{u}_1$ will also be orthogonal to the noise subspace. Stacking all these vectors as $\mathbf{U}_N = [\mathbf{u}_2 \quad \cdots \quad \mathbf{u}_m]$, the MUSIC method locates the break by searching for the location whose LFV is the most orthogonal to $\mathbf{U}_N$, i.e.,

$$\widehat{i} = \arg\max_i g(i) = \arg\max_i \frac{\mathbf{a}_i^T\mathbf{a}_i}{\mathbf{a}_i^T\mathbf{U}_N\mathbf{U}_N^T\mathbf{a}_i}, \tag{11}$$

where $\mathbf{a}_i$ is the LFV of a break at the i-th feasible location.

In summary, provided that a set of LFVs of the breaks at several feasible locations are available, the estimated location of the unknown break is found by observing the MUSIC spectrum, $g(i)$, as a function of these feasible locations and then finding its maximum; the location of the maximum is the estimated location for this unknown break.

3.3. Detailed procedures

The procedures for break localization with the MUSIC method are as follows.

MUSIC Algorithm for Break Localization

Preparation Stage (LFV database construction)

Obtaining N_p LFVs of the breaks having various sizes at several feasible locations uses (9). The details of the break events used in this study are provided in Table1.

Localization Stage

Let $\mathbf{X}$ represent the data block of an unknown break obtained by stacking the data from sensors of a type (e.g., pressure);

(1) Calculate the SVD of $\mathbf{X}$ and construct $\mathbf{U}_N$;

(2) $i = 1$;

(3) **Repeat**

(4) Calculate $g(i)$ using $\frac{\mathbf{a}_i^T\mathbf{a}_i}{\mathbf{a}_i^T\mathbf{U}_N\mathbf{U}_N^T\mathbf{a}_i}$;

(5) $i = i + 1$;

(6) **until** $i = N_p$;

(7) The location estimate of the unknown break is determined to be the location whose index $\widehat{i}$ having maximum $g(i)$.

4. Break size estimation

If a break is detected and localized, its size can be estimated using the proposed. deep learning model, as shown in Fig. 3. This convolutional neural network has alternating layers of different types resembling that of the AlexNet [28], with its input being an $m \times n$ data block. However, for applying AlexNet to break size estimation, it still needs to be modified as the original network is used for classification rather than regression for continuous values. Furthermore, the data block is formed by stacking the readings from the m selected sensors at n times. The only difference is that the selected sensors need not be of the same type. However, to mitigate the influence of magnitude imbalance in the readings of diversified sensors on estimation performance, we normalize each sensor's readings with its mean level under normal operation. Treating the multi-sensor data as an "image" (i.e., a two-dimensional data block) allows us to learn information using the framework of deep learning without handcrafted information extraction.

The convolution layers in the model shown in Fig. 3 are the core building blocks, used to extract useful information from the input data. Information extraction is achieved by convoluting the input data block with a set of learnable kernels/filters. Moreover, several "feature maps" that have different characteristics of the input data can be obtained [29,30]. The numbers of kernels/filters vary from 64 to 256 from one convolution layer to another, with all their sizes being 3×3. The outputs of convolution are passed through an element-wise rectified linear unit (ReLU) function. It is a nonlinear activation function that returns 0 if it receives any negative input; otherwise, it returns the input itself. The ReLU function is known for its capability to reduce the likelihood of the vanishing gradient problem and increase the speed of learning [31]. The interleaved max-pooling layers are used to down-sample the feature maps to

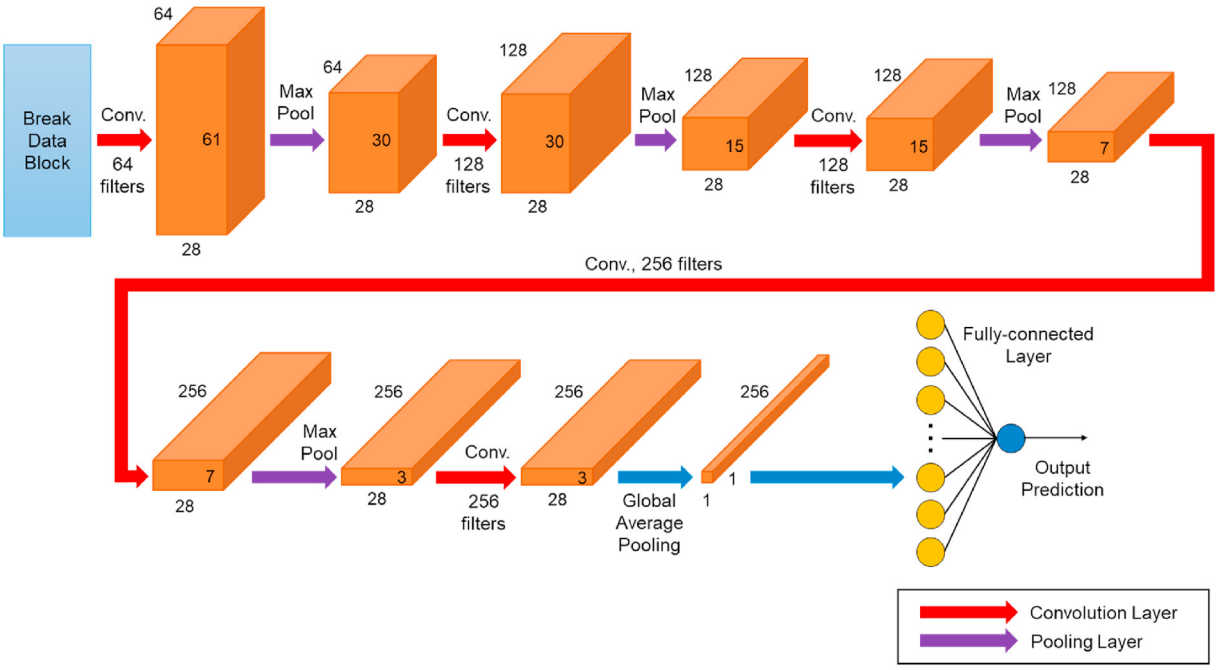

Fig. 3. The proposed deep learning model for break size estimation. This convolutional neural network has alternating layers of three types: convolution, pooling, and fully connected layers. The model input is a two-dimensional data block. The blocks following by different layers are the feature maps of various sizes.

be less sensitive to changes in the feature positions in the original map, known as "translation invariance" [32]. The pooling operation adopted in this study is max pooling, which extracts patches of size 1×2 from an input feature map and uses the maximum of these extracted features as their respective output. The size of the pooling operation allows a shift in the row direction of X owing to delayed detection of a break, due to high noise level. In a situation where the delay is significant, a larger size is chosen. As the selected sensors are not physically swapped, a shift in the column direction of X is not expected to occur, and thus a size of 1 is utilized. Unlike in the convolution layers, in pooling layers there is no learnable parameter. To regress the results of the convolution/pooling process for the break size, two more fully connected layers of 64 and 1 neurons are added. As the name implies, neurons in a fully connected layer have complete connections to all neurons in the previous layer. Finally, the activation function applied to the last fully connected layer (i.e., the output layer) is the identity activation function [33], and the activation function of the other fully connected layer is still the ReLU function. Before the fully connected layer, we use a global average pooling layer to flatten the output feature maps, which computes the mean value for each feature map (256 in total) from the last pooling layer and supplies the results to the following layer.

Finally, the kernels/filters in the convolution layers and the weights in the fully connected layers are determined by minimizing the size estimation error. In this study, we selected the mean absolute error as the loss function and used the adaptive moment estimation optimizer [21] to iterate on the N_p training break events for the optimal parameters. Note that these N_p events are the same as those for the LFV database construction.

5. Experiments and discussions

5.1. Data generation and parameter settings

Eighteen feasible break locations and six non-break event categories considered in this study are listed in Table 1 The LFVs of 336 break events at the eighteen locations were calculated using (9) to form the LFV database. The break sizes of.

Those belonging to LOCAs for constructing LFV database varied with constant intervals of 5 cm^2 and 100 cm^2 in the ranges of 5 cm^2–20 cm^2 (i.e., in the range of small break LOCAs according to the Maanshan final safety analysis report) and 100 cm^2–2000 cm^2, respectively. Another way to represent the break size of a LOCA is to normalize the size value by its possible maximum. This representation was also used in this study to express the break size of a LOCA. The possible maximum break sizes for an LOCA at the cold leg, hot leg, and crossover leg are 7664 cm^2, 8523 cm^2, and 9739 cm^2, respectively, according to the Maanshan operator training manual. The break sizes of those belonging to the main steam line break (MSLB) varied from 5 cm^2 to 2000 cm^2 with a constant interval of 100 cm^2. With regard to the steam generator tube rupture (SGTR), ten break sizes evenly spaced in the range between 5 cm^2 to 50 cm^2 were considered. Additionally, 550 break events whose sizes were randomly set in the same ranges were generated for evaluating the efficacy of the proposed methods. None of the breaks for performance evaluation had a size the same as those used for LFV database construction. For non-break events, three repetitions per class were simulated. Owing to the sensing noise (added later), any two event repetitions in any of these classes were not the same. All the simulations were performed in a

Table 1
Details of the breaks at 18 feasible locations and six non-break event categories used in this study. For a LOCA, the value in the parentheses is the normalized size.

Position Indices	Event Type	Break Position		Break Size Information
1	LOCA	Loop 1	Cold Leg	5 cm^2–2000 cm^2 (0.0652% ~ 26.0960%)
2			Hot Leg	5 cm^2–2000 cm^2 (0.0587% ~ 23.4659%)
3			Crossover Leg	5 cm^2–2000 cm^2 (0.0513% ~ 20.5360%)
4		Loop 2	Cold Leg	5 cm^2–2000 cm^2 (0.0652% ~ 26.0960%)
5			Hot Leg	5 cm^2–2000 cm^2 (0.0587% ~ 23.4659%)
6			Crossover Leg	5 cm^2–2000 cm^2 (0.0513% ~ 20.5360%)
7		Loop 3	Cold Leg	5 cm^2–2000 cm^2 (0.0652% ~ 26.0960%)
8			Hot Leg	5 cm^2–2000 cm^2 (0.0587% ~ 23.4659%)
9			Crossover Leg	5 cm^2–2000 cm^2 (0.0513% ~ 20.5360%)
10	MSLB	Loop 1		5–2000 cm^2
11		Loop 2		
12		Loop 3		
13	SGTR	Loop 1	Hot Leg Side of SG tubes	5–50 cm^2
14			Cold Leg Side of SG tubes	
15		Loop 2	Hot Leg Side of SG tubes	
16			Cold Leg Side of SG tubes	
17		Loop 3	Hot Leg Side of SG tubes	
18			Cold Leg Side of SG tubes	
Non-Break Events				
NB1	Main Steam Isolation Valve Failure (Loop 1)			
NB2	Main Steam Isolation Valve Failure (Loop 2)			
NB3	Main Steam Isolation Valve Failure (Loop 3)			
NB4	Loss of Main Feedwater			
NB5	Reactor Coolant Pump Trip			
NB6	All of Reactor Coolant Pump Trip			

simulator of Taiwan's Maanshan NPP, which is implemented using the Modular Accident Analysis Program Version 5 (MAAP5) [34]. Note that using the data produced by the computer codes such as MAAP5 for developing NPP online monitoring systems is not uncommon [3,6,35–37]. The advantage of utilizing these codes lies in their ability to simulate various LOCA and non-LOCA transients, lowering the burden of preparing relevant data while developing a monitoring system and allowing the researchers to concentrate more on proposing feasible algorithms. However, a modification is inevitable before applying these proposed schemes to a real NPP as the simulated data may deviate from those acquired in NPPs under an abnormal event of interest. The signals of 31 sensors covering four physical quantities were recorded under a sampling rate of 1 Hz. The details of these sensors are summarized in Table 2. A plant sensor was included for the analysis only when the sensing variable could be measured, and the sensor could appear in the NPP. To let the evaluation be realistic, sensing noise modeled as white Gaussian noise was added to each sensor's data. The noise level (i.e., σ_w) was specified by the signal-to-noise ratio defined as

$$\mathrm{SNR}_{\mathrm{dB}} = 20 \log_{10}\left(\frac{RMS(\mathbf{s}_{ij})}{\sigma_w}\right), \tag{12}$$

where $\mathrm{RMS}(\mathbf{s}_{ij})$ is the root-mean-square value of the data vector from the j^{th} sensor of the break event i. We set the SNR to be 40 dB. Finally, the network model for break size estimation was trained on TensorFlow 1.10.0 with the CUDA 9.0 Toolkit and cuDNN v7.3.1 on the computing platform: ASUS E500 G5 workstation with Intel Core™ i7-8700 CPU, GeForce RTX 2080, and 8 GB RAM. During training, a part of 336 break events (20% in this study) was

Table 2
List of the 31 sensors used in this study.

Sensor type	Sensor name	Unit
Water Level	S/G 1 downcomer water level	m
	S/G 2 downcomer water level	
	S/G 3 downcomer water level	
	Water level In pressurizer	
Pressure	Pressure in loop 1 S/G	Pa
	Pressure in loop 2 S/G	
	Pressure in loop 3 S/G	
	RCS pressure	
	Pressurizer pressure	
	Pressure in loop 1 hot leg	
	Pressure in loop 3 hot leg	
Temperature	Temperature of gas in pressurizer	K
	Temperature of water in pressurizer	
	Water temperature in loop 1 cold leg	
	Water temperature in loop 1 hot leg	
	Water temperature in loop 2 cold leg	
	Water temperature in loop 2 hot leg	
	Water temperature in loop 3 cold leg	
	Water temperature in loop 3 hot leg	
Flow Rate	Average flow in loop 1 cold leg	kg/s
	Average flow in loop 2 cold leg	
	Average flow in loop 3 cold leg	
	Water flow into loop 1 cold leg	
	Water flow into loop 2 cold leg	
	Water flow into loop 3 cold leg	
	Water flow into loop 1 hot leg	
	Water flow into loop 2 hot leg	
	Water flow into loop 3 hot leg	
	Water flow out from loop 1 hot leg	
	Water flow out from loop 2 hot leg	
	Water flow out from loop 3 hot leg	

considered as the validation set, and early stopping was used to halt the training to prevent overfitting. The batch size was 512.

5.2. Results and discussions

We first demonstrate the efficacy of Hotelling's T^2 test-based and the IQR-based approaches in detecting and isolating the testing events. As previously mentioned, an abnormal event is detected if the $T^2(t)$ value of any sensor type exceeds its corresponding T^2_α value. For a 0.01 significance level, the T^2_α values for the water level, pressure, temperature, and flow rate sensors were 9.5, 14.08, 15.53, and 21.06, respectively. The maximum differences between the occurrence and detection of a break (i.e., the detection times) are listed in Table 3. Comparing the event detection using the data vectors of different sensor types, we noticed that the pressure sensors were more sensitive in detecting the break events than other types of sensors.

Moreover, although the breaks occurred at different locations with different break sizes, they were all detected quickly. For example, a small break LOCA at Position 1 having size 15 cm^2 was

Table 3
Maximum detection times (s) of different abnormal events with different types of sensors and their corresponding scram times.

Position: 1					Position: 10				
Hotelling's T^2 test-based detection				Scram	Hotelling's T^2 test-based detection				Scram
W	P	T	F		W	P	T	F	
6	4	72	31	71	29	9	575	83	>1000
Position: 2					Position: 11				
Hotelling's T^2 test-based detection				Scram	Hotelling's T^2 test-based detection				Scram
W	P	T	F		W	P	T	F	
14	14	207	223	218	21	7	511	60	>1000
Position: 3					Position: 12				
Hotelling's T^2 test-based detection				Scram	Hotelling's T2 test-based detection				Scram
W	P	T	F		W	P	T	F	
7	5	81	24	85	49	19	191	271	>1000
Position: 4					Position: 13				
Hotelling's T^2 test-based detection				Scram	Hotelling's T^2 test-based detection				Scram
W	P	T	F		W	P	T	F	
7	5	87	106	100	29	32	394	469	432
Position: 5					Position: 14				
Hotelling's T^2 test-based detection				Scram	Hotelling's T^2 test-based detection				Scram
W	P	T	F		W	P	T	F	
7	5	100	108	102	19	18	158	222	214
Position: 6					Position: 15				
Hotelling's T^2 test-based detection				Scram	Hotelling's T^2 test-based detection				Scram
W	P	T	F		W	P	T	F	
8	9	117	119	114	20	20	352	357	214
Position: 7					Position: 16				
Hotelling's T^2 test-based detection				Scram	Hotelling's T^2 test-based detection				Scram
W	P	T	F		W	P	T	F	
7	5	74	55	95	15	12	165	174	166
Position: 8					Position: 17				
Hotelling's T^2 test-based detection				Scram	Hotelling's T^2 test-based detection				Scram
W	P	T	F		W	P	T	F	
7	3	112	35	104	24	25	315	375	368
Position: 9					Position: 18				
Hotelling's T^2 test-based detection				Scram	Hotelling's T^2 test-based detection				Scram
W	P	T	F		W	P	T	F	
12	7	135	166	162	13	13	172	170	163
Position: NB1					Position: NB2				
Hotelling's T^2 test-based detection				Scram	Hotelling's T^2 test-based detection				Scram
W	P	T	F		W	P	T	F	
3	4	30	7	>1000	2	3	27	9	>1000
Position: NB3					Position: NB4				
Hotelling's T^2 test-based detection				Scram	Hotelling's T^2 test-based detection				Scram
W	P	T	F		W	P	T	F	
3	4	31	8	>1000	5	21	81	50	86
Position: NB5					Position: NB6				
Hotelling's T^2 test-based detection				Scram	Hotelling's T^2 test-based detection				Scram
W	P	T	F		W	P	T	F	
5	4	17	1	4	5	4	16	1	4

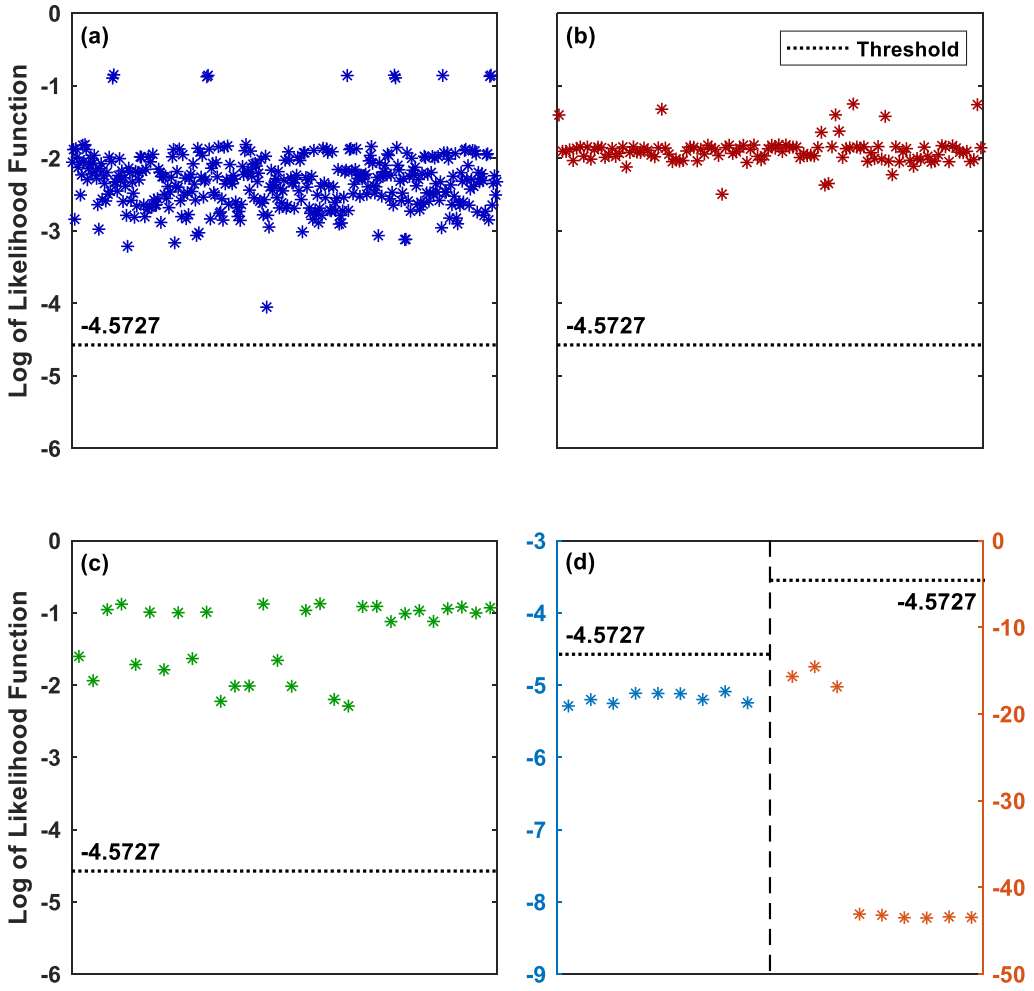

Fig. 4. Logarithm of the likelihood functions of 550 testing breaking events and 18 testing non-break events: (a) LOCA, (b) MSLB, (c) SGTR, and (d) non-break events.

detected in 4 s. This indicates that the continuous monitoring facilitates prompt break detection even when its size is small. The reactor scram times (concerning the break occurrence times) corresponding to these break events were also included for comparison. It is found that for almost all the events, the scram was triggered after their detection by Hotelling's T^2 test-based approach. Moreover, for some events (e.g., MSLBs at Positions 10, 11, and 12), the scram could not be triggered in 1000 s, which was the simulation period for each break event.

Next, the efficacy of the break isolation scheme was investigated. The feature vector used to represent an abnormal event was extracted using time integration from a 60-s data segment sensor-by-sensor. The data were also collected from the time Hotelling's T^2 test-based approach detected the event. The feature vectors $\mathbf{f}_i^B$ of the break events of interest, containing LOCAs, MSLBs, and SGTRs, were calculated similarly using the data of the events used for constructing the LFV database. We used a leave-one-out strategy to calculate the logarithm of the likelihood functions for evaluating the required parameters of the IQR-based isolation scheme, in which one of the feature vectors was selected as $\mathbf{f}$, and the likelihood function (4) was evaluated with the remaining feature vectors. The obtained IQR was 1.1615, resulting in a threshold of -4.5727. Finally, the smooth parameter was 0.08. We depict the logarithm of the likelihood functions of 550 testing break events and 18 non-break events in Fig. 4. As found, all the break events had their logarithm of the likelihood functions well above the threshold. On the contrary, those of the non-break events lay below the threshold so that they could be successfully excluded.

We now investigate the efficacy of the MUSIC method in locating a break in the NPP. Fig. 5 depicts the MUSIC spectra obtained using (11) when the breaks occur at the hot leg of loop 3 and the cold leg side of the steam generator tubes (loop 2). Fig. 5(a) is a favorable case, where a large peak in the spectrum is seen at index $i = 174$, corresponding to the location index of the unknown break (i.e., at the hot leg of loop 3). For (11) to hold, the LFV of the unknown break must occupy a subspace in the m-dimensional space that is completely different from those of the breaks at other feasible locations. However, this may not always hold. In practice, the signal subspaces of the breaks at different locations may not be as disjoint as in the previous example. This is particularly true when the two breaks are close to each other. Consequently, when the data block of a break that shares a common subspace with others is presented, the resulting MUSIC spectrum can lead to ambiguous results, as shown in Fig. 5(b), where the differences in the g(i) value of the correct location index and those of other locations become small. When this happens, the MUSIC method incorrectly locates the unknown break, although the index of the highest peak shown

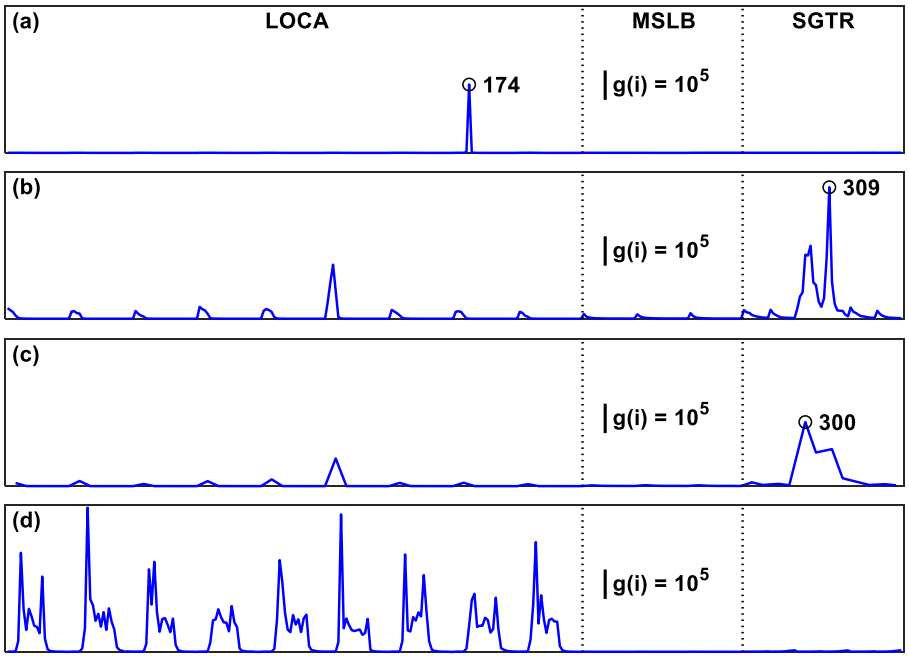

Fig. 5. The MUSIC spectra of different break events obtained using (11): (a) at the hot leg of loop 3, (b) at the cold leg side of the steam generator tubes (loop 2), (c) at the cold leg side of the steam generator tubes (loop 2) while working with a sparse LFV database, and (d) at the hot leg of loop 2 with the spectrum generated using the temperature data block.

Table 4
Accuracy of locating the 550 testing break events using the MUSIC method and the PNN-based approach.

Correctness Rate (%)			Size Interval		
			Original	Doubled	Quadrupled
MUSIC	Flow Rate	LOCA	99.73	99.19	95.41
		MSLB	100	97.5	95
		SGTR	96.67	91.67	68.33
	Pressure	LOCA	31.89	26.76	21.35
		MSLB	100	100	98.33
		SGTR	58.33	53.33	43.33
	Temperature	LOCA	32.16	32.43	25.68
		MSLB	100	99.17	95
		SGTR	45	45	43.33
	Water Level	LOCA	14.05	13.78	15.14
		MSLB	93.33	90	71.67
		SGTR	70	61.67	48.33
PNN	Flow Rate	LOCA	94.86	94.05	84.32
		MSLB	51.67	51.67	51.67
		SGTR	65	66.67	65
	Pressure	LOCA	47.84	40	34.59
		MSLB	51.67	51.67	51.67
		SGTR	60	55	36.67
	Temperature	LOCA	37.03	34.32	30.54
		MSLB	51.67	51.67	51.67
		SGTR	21.67	25	21.67
	Water Level	LOCA	17.57	17.03	13.51
		MSLB	41.67	40.83	31.67
		SGTR	65	61.67	66.67
	All	LOCA	91.62	85.95	78.38
		MSLB	51.67	51.67	51.67
		SGTR	65	70	63.33

in Fig. 5(b) still corresponds to the unknown break ($i = 309$). We summarize the results of locating the 550 testing breaks using the MUSIC method in Table 4. We also include the localization results using the pattern recognition-based approach of Na et al. (2004) [6] for comparison, where a probabilistic neural network (PNN) classifies the event features extracted by the integrator to determine the location of a break. The reactor scram was adopted to indicate an event (also functions as the starting time of integration). The data duration for each sensor was still 60 s (i.e., $n = 61$). The studies of event identification (e.g. Refs. [6,7]) also comprise selecting a 60-s duration. In these studies, a 60-s duration was selected, after the reactor scram, as safety systems, such as the safety injection system

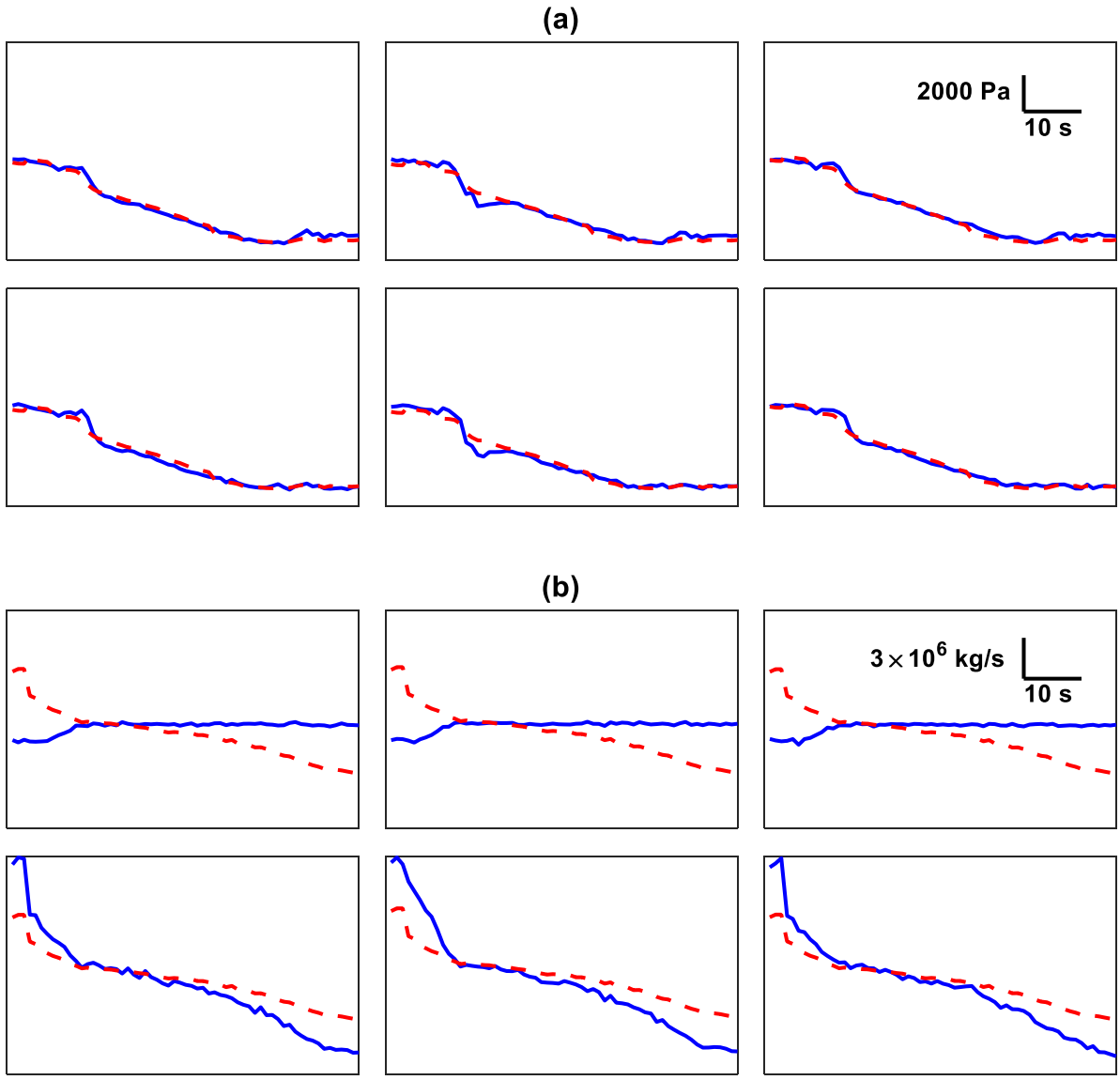

Fig. 6. The data blocks (blue solid lines) of a LOCA occurred at the hot leg of loop 1 and its reconstructed noise-free signals $\hat{\mathbf{a}}\hat{\mathbf{v}}^T$ (red dashed lines). (a) Flow rate data block and (b) Pressure data block.

and auxiliary feedwater system, were not actuated. We followed their setting in this study. As can be seen, using the MUSIC method with the data blocks of flow rate, almost all the break events could be correctly located regardless of their locations and sizes. We also noticed that when the two breaks were close to each other, the pattern recognition-based approach could not distinguish them, indicating that this approach is error-prone (e.g., misclassifying a break at the cold leg side of the steam generator tubes as at the hot leg side of the steam generator tubes). Furthermore, the accuracy for locating the MSLBs using the PNN-based approach was low because a small MSLB could not trigger a scram in the simulation period; hence, the subsequent localization step was not activated. This also demonstrated the significance of an adequate detection scheme in break event mitigation. Furthermore, only when the sensors of all types were considered simultaneously, the PNN-based approach presented an acceptable localization accuracy. However, if two breaks are not only close to each other but also of small sizes, the MUSIC method might still incorrectly locate them. For example, the errors made by the MUSIC method were incorrectly locating a small break LOCA at the crossover leg of loop 3 as SGTR at the hot leg side of steam generator tubes (loop 3) (i.e., locating a break event belonging to Class 9 as Class 17) or an SGTR at the hot leg side of steam generator tubes to be at the cold leg side of steam generator tubes (i.e., locating a break event belonging to Class 15 as Class 16). The proximity of these breaks and their small sizes caused the LFVs of the breaks to be nearly the same, as shown in Fig. 2(c), thus making the localization using the MUSIC method difficult. However, the same difficulty was also seen in the PNN-based approach.

As mentioned earlier, breaks of different sizes may have different LFVs (e.g., those shown in Fig. 2(b)) even when they are at the same location. Thus, when building up the LFV database, the size of a break at a given location should be varied to factor this. The break sizes used during the database construction were evenly

Table 5
Mean residuals and mean relative errors for the size estimation of 550 testing break events. Three size intervals were used. For a LOCA, the value in the parentheses is the normalized size.

Size Interval		Original Setting		Doubled		Quadrupled	
Event Info.							
Event Type	Pos. No.	Residual (cm^2)	Re. Err. (%)	Residual (cm^2)	Re. Err. (%)	Residual (cm^2)	Re. Err. (%)
LOCA	1	19.46 (0.2539%)	2.67	38.43 (0.5014%)	9.40	82.60 (1.0778%)	25.26
	2	11.43 (0.1341%)	1.29	18.00 (0.2112%)	2.17	46.94 (0.5508%)	7.76
	3	9.22 (0.0947%)	1.99	14.94 (0.1534%)	3.48	37.84 (0.3885%)	14.23
	4	18.72 (0.2443%)	4.71	44.07 (0.5751%)	11.17	73.51 (0.9592%)	27.03
	5	18.41 (0.2160%)	2.19	23.10 (0.2710%)	6.05	54.24 (0.6364%)	20.02
	6	9.48 (0.0974%)	1.29	12.65 (0.1229%)	1.99	42.74 (0.4389%)	9.46
	7	19.51 (0.2546%)	1.99	29.57 (0.3858%)	6.06	60.08 (0.7840%)	20.89
	8	27.03 (0.3172%)	2.85	40.50 (0.4752%)	8.53	125.40 (1.4713%)	47.29
	9	14.68 (0.1507%)	4.11	18.16 (0.1865%)	4.53	40.37 (0.4146%)	16.32
MSLB	10	8.94	1.17	16.41	5.50	31.60	8.46
	11	11.67	1.51	18.76	3.94	60.07	15.29
	12	13.94	4.93	23.47	7.81	49.04	12.12
SGTR	13	0.48	1.23	1.09	5.03	8.35	26.06
	14	0.44	2.06	0.75	3.29	5.36	27.91
	15	0.42	3.99	0.97	7.11	4.94	33.94
	16	0.49	2.75	1.71	10.60	5.09	35.58
	17	0.28	1.82	1.03	8.19	5.20	28.65
	18	0.44	1.68	2.11	8.67	9.57	39.53

spaced; however, the adopted size interval affected the localization accuracy. To illustrate how the localization accuracy was influenced, we doubled and quadrupled the intervals to reconstruct two sparse LFV databases for the test. Note that only 168 and 81 break events remained after doubling and quadrupling the size intervals. We list the localization results using these two sparse LFV databases in Table 4. The advantage of working with the sparse LFV databases was that an unknown break could be located only in half or one-fourth of the time originally required. However, the localization accuracy reduced as the size interval increased, as shown in Table 4. The errors increased owing to incorrectly locating nearby breaks as the discriminant power of the MUSIC method reduced when working with the sparse LFV databases. This was particularly true when locating SGTRs, with the success rate being as low as 68.33% using the flow rate data blocks. Fig. 5(c) shows the MUSIC spectrum using the sparse LFV database. The test break event was the same as that in Fig. 5(b). However, the highest peak in this case appeared at index $i = 300$ rather than at $i = 309$, indicating incorrect localization. Therefore, factors (i.e., break location and size) that affect the LFVs must be carefully considered for the MUSIC method to be efficacious.

Finally, with the data blocks of other sensor types, the MUSIC method performed ineffectively, as shown in Table 4. To verify the reason for this poor performance, the correctness of the rank-one assumption for these data blocks was assessed. If the assumption holds, the break data block should be similar to the estimated noise-free signals, $\widehat{\mathbf{a}}\widehat{\mathbf{v}}^T$. This is seen in Fig. 6(a), where the estimated noise-free signals (i.e., red dashed lines) are nearly on top of the flow rate data block (i.e., the blue solid lines) of a LOCA at the hot leg of loop 1. This trend was also found in the flow rate data blocks of other break events. In other sensor types, significant deviations between the data blocks and their rank-one noise-free signals could be seen, as shown in Fig. 6(b). Because of this violation of the assumption, the LFVs of a break obtained using (9) could not well represent the break, and the resulting MUSIC spectrum became "spiky" (e.g., the spectrum obtained using the temperature block shown in Fig. 5(d)), causing poor localization accuracy.

We finally evaluated the efficacy of the proposed deep learning model for break size estimation. The model input was the data block composed of the normalized readings from all the sensors regardless of their types. The data duration used for estimation was still 60 s. Note that the break events used to train the size estimation models for the 18 break event categories were the same as those for the LFV database construction. For each event category, the training process was repeated ten times for ten different model realizations. When an unknown break was located, its corresponding ten models were used to estimate its size. The residual, pull (i.e., residual/model uncertainty) and relative error were employed to quantify the estimation performance of these models [38,39], where the error was defined as the absolute difference between the actual and estimated sizes. We summarize the size estimation results for the 550 testing break event in Table 5. The maximum mean residual was 27.03 cm^2 (0.3172%) for a LOCA that occurred at the hot leg of loop 3. The value in the parentheses is its normalized size. Although this residual appeared to be significant, the corresponding mean relative error was 2.85%. Based on the size estimation results of LOCAs shown in Fig. 7, we observed that the residual increased with the break size, whereas the relative errors decreased. From the cumulative distribution function (CDF) of their relative errors, we noticed that more than 95% of the testing events had relative errors less than 8%. Those having relative errors of

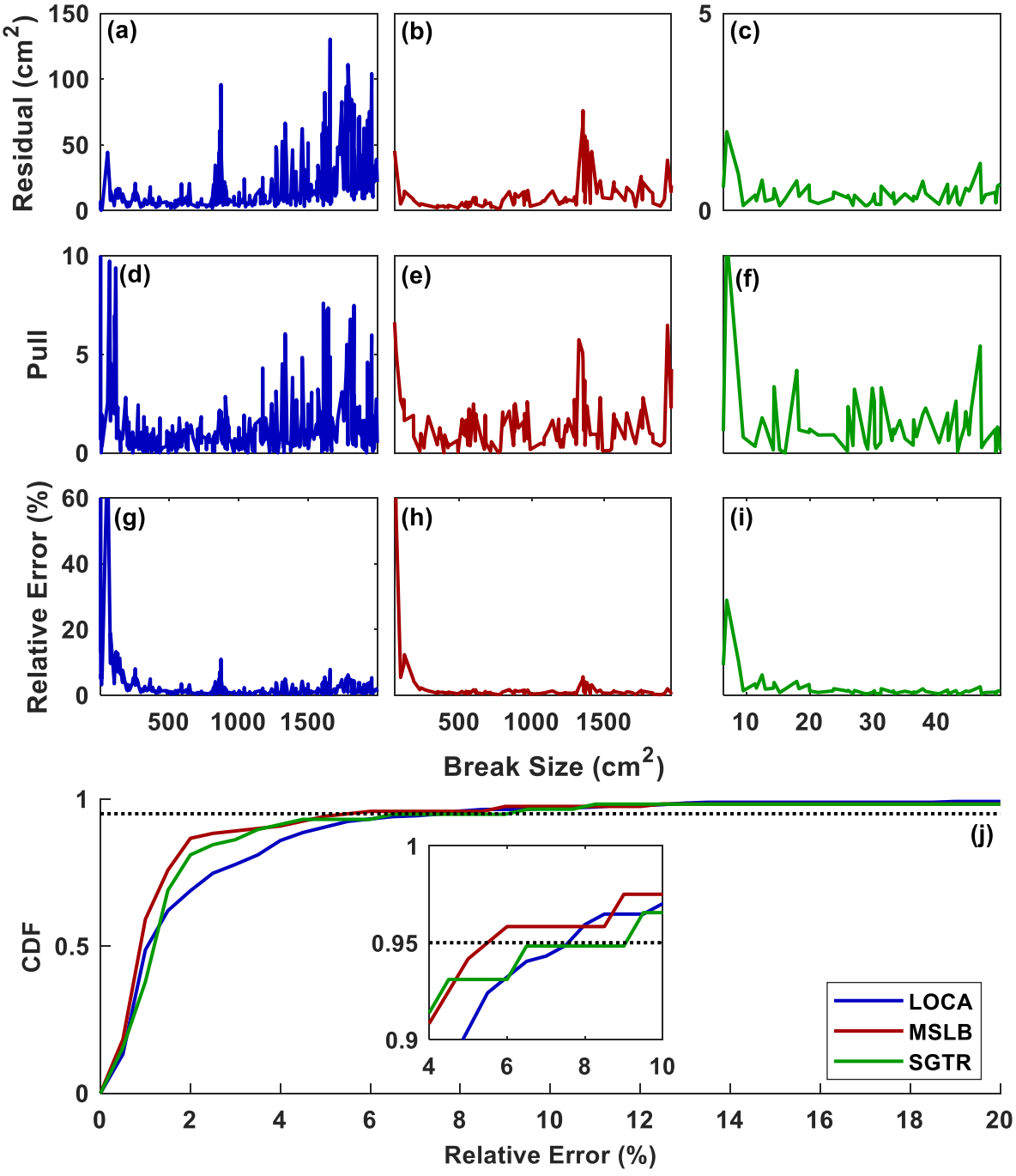

Fig. 7. Size estimation residuals, pulls, and relative errors for various break events. LOCA: (a), (d) and (g). MSLB: (b), (e) and (h). SGTR: (c), (f) and (i). Cumulative distribution functions (CDFs) of relative errors: (j).

more than 8% were owing to the estimation of LOCAs with small sizes. This is reasonable because a small estimation error can lead to a significant relative error when the actual size is small. In contrast, a significant estimation error can only result in a small relative error when the actual break size is large. Finally, for some of the break events, the pulls were significant as their ten size estimation models could provide size estimation results with limited variances. For the break events of MSLB and SGTR, the situations were similar, as shown in Fig. 7. The maximum mean residuals for these two event categories were 13.94 cm^2 and 0.49 cm^2, respectively. As for the mean relative errors, the maximum values were 4.93% and 3.99%, respectively, as listed in Table 5. Furthermore, doubling or quadrupling the size interval also led to increases in estimation errors as the break events available for training the size estimation models were reduced; hence, it was not easy to obtain applicable models in those circumstances.

Table 6
Size estimation performance of the proposed approach and the SVR method. For a LOCA, the value in the parentheses is the normalized size.

Size Estimation Methods	Proposed Approach	SVR		
Detection Methods	Hotelling's T^2 test	Reactor Scram		Hotelling's T^2 test
Localization Methods	MUSIC	PNN	Localized Correctly	Localized Correctly
	Mean Residual (cm^2)			
LOCA	16.44	145.00	129.17	126.82
	(0.1959%)	(1.7472%)	(1.5411%)	(1.5101%)
MSLB	11.52	121.86	121.86	119.31
SGTR	0.42	5.30	3.51	3.53
	Mean Relative Error (%)			
LOCA	2.30	33.39	29.12	28.29
MSLB	2.54	10.31	10.30	8.76
SGTR	2.26	34.41	23.28	23.43

Additionally, we implemented the break size estimation approach of Na et al. (2008) [3] for comparison wherein, to regress the event features extracted by the integrator for the break size, a support vector regression (SVR) model was used. Note that the features used for model training were the same as those for training the PNN classifier for break localization presented previously, and 18 size estimation models were obtained for the 18 break event categories. If PNN located the unknown break, its corresponding model was used to estimate the break size. Table 6 summarizes the size estimation performance of the proposed scheme and the SVR model. The results of estimating 550 testing breaks were divided into three categories (LOCA, MSLB, and SGTR), whose mean residual and mean relative error were calculated accordingly. As can be seen, the mean residual and mean relative error of SVR were larger than those of the proposed approach regardless of the event categories. Three possible reasons for the poor performance of the SVR method are as follows. First, a wrong size estimation model was adopted due to incorrectly locating the break by PNN. To verify this, we evaluated each break with its corresponding size estimation SVR model (i.e., assuming that the break event was localized correctly). The mean residuals and mean relative errors of the different event types decreased, as shown in Table 6. Second, the data used for feature extraction were collected after the reactor scram for 60 s in Ref. [3]. In this period, the sensing readings varied less. The features in input data that help estimate the break size were thus less informative, leading to poor estimation results. This was demonstrated by estimating the break size using the data considered after detecting the break using Hotelling's T^2 test-based scheme, and the errors were further decreased, as shown in Table 6. Lastly, the integrator was a low pass filter, and the information that could help estimate the break size was substantially discarded after feature extraction. Thus, the errors in the break size estimation were still significant.

Finally, we summarize the strengths and weaknesses of this work as follows:

- Instead of using the reactor scram as an indicator for the occurrence of an abnormal event, Hotelling's T^2 test-based approach simultaneously monitored changes in the readings of multiple NPP sensors to attain prompt event detection. Moreover, having the logarithm of their likelihood functions well above the preset threshold determined by the IQR method, the break events were correctly isolated for localization.
- The MUSIC method was able to distinguish two close breaks (e.g., LOCAs at the cold and hot legs of any loop), which was difficult to attain using the PNN-based approach. However, if two breaks were not only close to each other but also of small sizes, the MUSIC method might still wrongly locate them. Unlike the PNN-based approach, whose discriminant power is dictated by the extracted features, the discriminant power of the MUSIC method comes from the LFV database. Therefore, factors that affect the LFVs must be carefully considered for the MUSIC method to be efficacious.
- The break sizes estimated by the proposed deep learning model were close to the actual values, having estimation errors less than those obtained using the SVR-based method. Furthermore, information extraction in the proposed model is achieved by convoluting the input data block with a set of learnable kernels/filters without the need for handcrafted feature extraction. However, the estimation of small-size breaks had relative errors of more than 8%, which requires an alternative approach to address.

6. Conclusion

Several algorithms that enable detection, isolation, localization, and size estimation of breaks in NPPs were presented, with their performance being evaluated using the data generated by a simulator in Taiwan's Maanshan NPP. Based on Hotelling's T^2 test and the IQR-based isolation scheme, it was observed that a break event could be promptly detected by simultaneously monitoring the changes in the readings of multiple NPP sensors and isolating before localization. For a test of 18 break event categories with a total of 550 testing events, the MUSIC method achieved a success rate of at least 96.67% for break location. Two closely located breaks could be distinguished by employing the MUSIC method; however, mislocalization could happen if they were close and of small sizes. In addition, since the discriminant power of the MUSIC method comes from the LFV database, factors that affect the LFVs must be appropriately considered. Owing to the ability of a deep learning model to adapt itself to the shape of the available data, the break size estimates came closer to their actual values. Although the mean relative error obtained while estimating the testing breaks' sizes using the proposed network model was less than 4.93%, the size estimates of the small-size breaks had relative errors of more than 8%, leading to the need for an alternative approach to address this issue.

Declaration of competing interest

The authors declare that they have no known competing financial interests or personal relationships that could have appeared to influence the work reported in this paper.

References

[1] C. Queral, J. González-Cadelo, G. Jimenez, E.J.N.T. Villalba, Accident

management actions in an upper-head small-break loss-of-coolant accident with high-pressure safety injection failed, Nucl. Technol. 175 (2011) 572–593.
[2] J. Montero-Mayorga, C. Queral, J. Gonzalez-Cadelo, Effects of delayed RCP trip during SBLOCA in PWR, Ann. Nucl. Energy 63 (2014) 107–125.
[3] M.G. Na, W.S. Park, D.H. Lim, Detection and diagnostics of loss of coolant accidents using support vector machines, IEEE Trans. Nucl. Sci. 55 (2008) 628–636.
[4] S.-J. Lee, J. Kim, S.-C. Jang, Human error mode identification for NPP main control room operations using soft controls, J. Nucl. Sci. Technol. 48 (2011) 902–910.
[5] T. Santosh, G. Vinod, R. Saraf, A. Ghosh, H. Kushwaha, Application of artificial neural networks to nuclear power plant transient diagnosis, Reliab. Eng. Syst. Saf. 92 (2007) 1468–1472.
[6] M.G. Na, S.H. Shin, S.M. Lee, D.W. Jung, S.P. Kim, J.H. Jeong, B.C. Lee, Prediction of major transient scenarios for severe accidents of nuclear power plants, IEEE Trans. Nucl. Sci. 51 (2004) 313–321.
[7] Y.-G. No, J.-H. Kim, M.-G. Na, D.-H. Lim, K.-I. Ahn, Monitoring severe accidents using AI techniques, Nucl. Eng. Technol. 44 (2012) 393–404.
[8] M. Saghafi, M.B. Ghofrani, Real-time estimation of break sizes during LOCA in nuclear power plants using NARX neural network, Nucl. Eng. Technol. 51 (2019) 702–708.
[9] T. Santhosh, M. Kumar, I. Thangamani, A. Srivastava, A. Dutta, V. Verma, D. Mukhopadhyay, S. Ganju, B. Chatterjee, V. Rao, A diagnostic system for identifying accident conditions in a nuclear reactor, Nucl. Eng. Des. 241 (2011) 177–184.
[10] X. Tian, V. Becerra, N. Bausch, T. Santhosh, G. Vinod, A study on the robustness of neural network models for predicting the break size in LOCA, Prog. Nucl. Energy 109 (2018) 12–28.
[11] L.H. Chiang, E.L. Russell, R.D. Braatz, Fault Detection and Diagnosis in Industrial Systems, Springer Science & Business Media, 2000.
[12] B.M. Wise, N.B. Gallagher, The process chemometrics approach to process monitoring and fault detection, J. Process Contr. 6 (1996) 329–348.
[13] S.-C. Wu, K.-Y. Chen, T.-H. Lin, H.-P. Chou, Multivariate algorithms for initiating event detection and identification in nuclear power plants, Ann. Nucl. Energy 111 (2018) 127–135.
[14] J.-D. Lin, W.-H. Fang, Y.-Y. Wang, J.-T. Chen, FSF MUSIC for joint DOA and frequency estimation and its performance analysis, IEEE Trans. Signal Process. 54 (2006) 4529–4542.
[15] B. Friedlander, A.J. Weiss, Direction finding using spatial smoothing with interpolated arrays, IEEE Trans. Aero. Electron. Syst. 28 (1992) 574–587.
[16] S.-C. Wu, A.L. Swindlehurst, P.T. Wang, Z.Z. Nenadic, Projection versus prewhitening for EEG interference suppression, IEEE T. Bio-Med. Eng. 59 (2012) 1329–1338.
[17] R. Schmidt, Multiple emitter location and signal parameter estimation, IEEE Trans. Antenn. Propag. 34 (1986) 276–280.
[18] G.S. Babu, P. Zhao, X.-L. Li, Deep convolutional neural network based regression approach for estimation of remaining useful life, in: International Conference on Database Systems for Advanced Applications, Dalas, U. S. A, 2016. April 16-19.
[19] L.K. Tan, Y.M. Liew, E. Lim, R.A. McLaughlin, Convolutional neural network regression for short-axis left ventricle segmentation in cardiac cine MR sequences, Med. Image Anal. 39 (2017) 78–86.
[20] S. Lathuilière, P. Mesejo, X. Alameda-Pineda, R. Horaud, A comprehensive analysis of deep regression, IEEE T. pattern anal. 42 (2019) 2065–2081.
[21] D.P. Kingma, J. Ba, Adam, A Method for Stochastic Optimization, 2014 arXiv preprint arXiv:1412.6980.
[22] M.J. Embrechts, S. Benedek, Hybrid identification of nuclear power plant transients with artificial neural networks, IEEE Trans. Ind. Electron. 51 (2004) 686–693.
[23] S.G. Vinod, A. Babar, H. Kushwaha, V.V. Raj, Symptom based diagnostic system for nuclear power plant operations using artificial neural networks, Reliab. Eng. Syst. Saf. 82 (2003) 33–40.
[24] D.C. Montgomery, G.C. Runger, Applied Statistics and Probability for Engineers, John Wiley & Sons, 2010.
[25] J. Han, J. Pei, M. Kamber, Data Mining: Concepts and Techniques, Elsevier, 2011.
[26] B.W. Silverman, Density Estimation for Statistics and Data Analysis, CRC Press, 1986.
[27] T.K. Moon, W.C. Stirling, Mathematical Methods and Algorithms for Signal Processing, Prentice Hall, 2000.
[28] A. Krizhevsky, I. Sutskever, G.E. Hinton, Imagenet classification with deep convolutional neural networks, Adv. Neural Inf. Process. Syst. 25 (2015) 1097–1105.
[29] A. Krizhevsky, I. Sutskever, G.E. Hinton, Imagenet classification with deep convolutional neural networks, in: Twenty-sixth Conference on Neural Information Processing Systems, Stateline, U. S. A., 2012. December 3-8.
[30] Y. LeCun, Y. Bengio, G.E. Hinton, Deep learning, nature 521 (2015) 436–444.
[31] G.E. Dahl, T.N. Sainath, G.E. Hinton, Improving deep neural networks for LVCSR using rectified linear units and dropout, in: IEEE International Conference on Acoustics, Speech and Signal Processing, Vancouver, Canada, 2013. May 26-31, 2013.
[32] M. Jaderberg, K. Simonyan, A. Zisserman, K. Kavukcuoglu, Spatial transformer networks, in: Twenty-ninth Conference on Neural Information Processing Systems, Montréal, Canada, 2015. December 7-10.
[33] T. Shimobaba, T. Kakue, T. Ito, Convolutional neural network-based regression for depth prediction in digital holography, in: IEEE 27th International Symposium on Industrial Electronics (ISIE), Cairns, Australia, 2018. June 13-15, 2018.
[34] T. Kindred, Modular Accident Analysis Program 5 (MAAP5) Applications Guidance: Desktop Reference for Using MAAP5 Software—phase 3 Report, Electric Power Research Institute, 2017.
[35] C. Gottlieb, V. Arzhanov, W. Gudowski, N. Garis, Feasibility study on transient identification in nuclear power plants using support vector machines, Nucl. Technol. 155 (2006) 67–77.
[36] K.H. Yoo, Y.D. Koo, J.H. Back, M.G. Na, Identification of LOCA and estimation of its break size by multiconnected support vector machines, IEEE Trans. Nucl. Sci. 64 (2017) 2610–2617.
[37] K.H. Yoo, J.H. Back, M.G. Na, S. Hur, H. Kim, Smart support system for diagnosing severe accidents in nuclear power plants, Nucl. Eng. Technol. 50 (2018) 562–569.
[38] K. Moshkbar-Bakhshayesh, Development of a modular system for estimating attenuation coefficient of gamma radiation: comparative study of different learning algorithms of cascade feed-forward neural network, J. Instrum. 14 (2019), 10010.
[39] K. Moshkbar-Bakhshayesh, Bayesian regularization of multilayer perceptron neural network for estimation of mass attenuation coefficient of gamma radiation in comparison with different supervised model-free methods, J. Instrum. 15 (2020), 11019.